Boundary Tension at the Interface of Nanoscopic Helium Films on an Heterogeneous Substrate

E. S. Hernández

Journal of Low Temperature Physics

ISSN 0022-2291

J Low Temp Phys
DOI 10.1007/s10909-014-1143-3

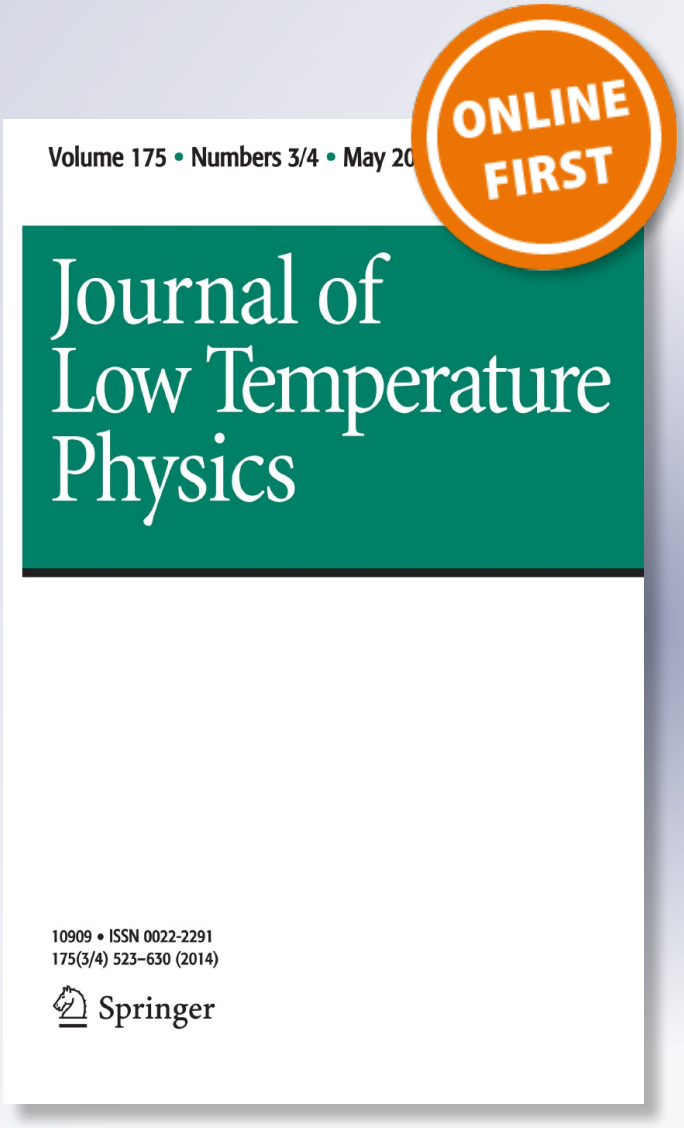

Springer

J Low Temp Phys
DOI 10.1007/s10909-014-1143-3

Boundary Tension at the Interface of Nanoscopic Helium Films on an Heterogeneous Substrate

E. S. Hernández

Received: 7 November 2013 / Accepted: 17 February 2014

Abstract This paper reports the first calculation of the two-dimensional interfacial profile and energetics of nanoscopically thin films of helium, on an heterogeneous planar substrate consisting of two adjoining metals. The calculations are performed in the frame of density functional theory at zero temperature, with the purpose of identifying the formation process of the interface at the boundary between the two substrates when few atomic layers are involved, to elucidate the possible relationship of the magnitude of the boundary tension with the displacement of layers between the half films, and to extract keys to organize future calculations of film coexistence at finite temperatures.

Keywords Helium films · Heterogenous substrates · Interfacial tension

PACS 05.30.Jp · 05.70.Np · 67.25.bh · 67.60.gj

1 Introduction

Wetting transitions involving a vapor (v), a liquid (l) and a solid (s) component, take place when it becomes energetically more convenient to build two interfaces than three (see e.g., the reviews in Ref. [1–3]). As the spreading power $S(T) = \sigma_{sv}(T) - \sigma_{sl}(T) - \sigma_{lv}(T)$, with σ_{ij} the interfacial tension between phases i and j, becomes positive

E. S. Hernández
Departamento de Física, Facultad de Ciencias Exactas y Naturales, Universidad de Buenos Aires, Buenos Aires, Argentina

E. S. Hernández (✉)
Instituto de Física de Buenos Aires, Consejo Nacional de Investigaciones Científicas y Técnicas, Buenos Aires, Argentina
e-mail: shernand@df.uba.ar

Published online: 12 March 2014

as a function of temperature T, a liquid phase of macroscopic thickness interposes uniformly between solid and vapor. A byproduct of first order wetting transitions is the appearance of a prewetting (PW) line [4,5] in thermodynamic phase space, extending in a range of temperatures $T_W \leq T \leq T_{PW}$ and characterized by coexistence of a thin and a thick liquid film on the solid surface, at a chemical potential $\mu(T)$ lower than the saturation one $\mu_0(T)$ for liquid–vapor equilibrium at the given temperature.

In this case, the thermodynamic phase diagram $\Delta\mu = \mu - \mu_0$ vs T splits into two regimes: (a) the low temperature ($T < T_W$), partial wetting (PaW) one characterized by the presence of spherical liquid casks on a thin liquid film on the solid surface, surrounded by a circular contact line of microscopic width, and characterized by a contact angle θ defined by Young's relation $\cos\theta = (\sigma_{sv} - \sigma_{sl})/\sigma_{lv}$, and (b) the PW coexistence region. As one approaches T_W from below, the microscopic contact line evolves into a macroscopic transition zone, translationally invariant along one direction parallel to the substrate, that situates the one-dimensional (1D) interface between the thin and the thick film. Consequently with these geometries, in either side of the first order wetting transition the free energy excess with respect to the bulk systems acquires a contribution per unit length. The energy cost due to the inhomogeneity is the line tension (τ) in the PaW region, and the boundary tension (τ_b) along the PW line [6]. These quantities, like the surface tension at the two-dimensional (2D) interface between two bulk phases, are thermodynamically well defined and must coincide as one approaches the wetting transition form either side.

The existence of this interfacial energy cost, a consequence of energy and entropy imbalance among the particles in the different phases that meet at the contact line, was recognized by Gibbs in his pioneering papers [7], and triggered many studies along various decades. Several theoretical analyses [8,9] (see also the review in Ref. [10]) establish that the behavior of τ near T_W depends crucially on the order of the wetting transition and on the range of the intermolecular forces. From the experimental viewpoint, the relatively small magnitudes of τ, in the range 10^{-12} to 10^{-5} N for classical fluids (1 N = 7.24 10^{12} K/Å in the units adopted hereafter), calls for very accurate techniques to view and measure the contact angle, together with a smooth and homogeneous solid surface and a highly purified liquid [11].

A closely related subject is the structure of the interface occuring at the edge of inhomogeneities on a chemically patterned substrate, consisting of one or more different materials. The understanding of these interfaces and their energetics may be crucial for technological uses such as coating and microfluidic circuits, where the patterned surface can be tuned to control wettability, as well as many other physical and biological applications [12]. Some examples of such substrates are striped surfaces with alternating wettable and nonwettable adsorbers with respect to a given fluid [13–15] or circular lyophobic domains embedded in a lyophilic matrix [13,16]. The simplest realization of such a substrate, wetted by helium, has been presented in Ref. [17] in the frame of a phenomenological model. In this case, the subspace $z > 0$ splits into two halves containing different solids for $x < 0$ and for $x \geq 0$, keeping translational invariance along the y–axis.

On the other hand, classical density functional theory [18] has proved to be a valuable tool to compute the boundary tension within a mean field description [19]. As in Ref. [17], in the latter work the authors explore the shape of the interface between the

left and right adsorbed films. This approach permits to show that interfacial Hamiltonian models [10], which allow to obtain the border $z = l(x)$ between a liquid film and the equilibrium vapor by functional differentiation of the boundary tension [8,9], can be rigorously derived from the energy density kernel, both in their nonlocal and local versions [19,20]. Although the predictions of the nonlocal theory originally predicted a much broader transition region than the local displacement model, later refinements of the numerical techniques [21] permitted to establish that while both theories provide equivalent descriptions, the more accurate nonlocal theory is necessary when the interfacial profiles exhibit large curvatures.

The purpose of this work is to investigate the structure and energetics of the two-dimensional interfacial profile between the half–films of liquid ^{4}He on a chemically heterogeneous substrate consisting of two metals. With Cs as an exception, at zero temperature ^{4}He wets Mg and alkali metals, with prewetting jumps of a few atomic layers [24]; consequently, one may address the particular problem of films of nanoscopic spread, which *a priori* may lie outside the domain of application of interfacial models due to their noticeable shell structure. As shown along this work, the small number of helium layers participating in the construction of the interface makes room to new energetic aspects, such as the possible relation between the sign of the boundary tension and the displacement of matter along the interface to remove or add single monolayers.

The calculations are performed resorting to a finite temperature–finite range density functional [22] (FRDF) that permitted to perform detailed calculations of adsorption isotherms of ^{4}He on semiinfinite planar alkali metals [23], and allowed to establish the density profiles of the coexisting thin and thick films on Cs, the wetting temperature T_W at 2.1 K, in good agreement with experimental observations, and the PW line up to 3 K.[1] For this sake, Sect. 2 briefly describes the FRDF formalism and the numerical approach. The calculations and results are described in Sect. 3 and summarized in Sect. 4.

2 Two Film Coexistence Within FRDF

Since the formalism and peculiarities of the FRDF employed in this work have been given in many references [25], most details are skipped here in order to call attention on the general background. The determination of the density profiles $\rho(\mathbf{r})$ and energetics of the films is obtained by solving a three-dimensional (3D) nonlinear, integrodifferential Euler–Lagrange (EL) equation for the wave function $\Psi = \sqrt{\rho}$ of the helium atoms of mass m of the form

$$\left\{ -\frac{\hbar^2}{2m} \nabla^2 + V\left[\rho(\mathbf{r})\right] + V_s(z) \right\} \Psi(\mathbf{r}) = \mu \, \Psi(\mathbf{r}) \tag{1}$$

[1] In fact, FRDF theory is unable to match the prewetting temperature T_{PW} at the expected experimental figure of ≈2.5 K, due to the limitations of mean field theory in accounting for critical phenomena.

constructed by functional differentiation $\delta\Omega/\delta\rho = 0$ of a thermodynamic grandpotential

$$\Omega = \int d\mathbf{r}\ \{\mathscr{F}[\rho(\mathbf{r})] + [V_s(z) - \mu]\ \rho(\mathbf{r})\} \tag{2}$$

where $\mathscr{F}[\rho]$ is a temperature–dependent free energy density[22], μ is the chemical potential of the helium atoms and V_s the substrate field. In this work, the adsorbing surface is composed by one right (R) and one left (L) adsorber joined at the line $x = 0$, so that adhesive forces derive from a step–wise potential [17]

$$V_s(x, z) = V_R(z)\,\Theta(-x) + V_L(z)\,\Theta(x) \tag{3}$$

with $\Theta(x)$ the usual step function, and with $V_{R,L}$ the potential offered to the helium atoms by homogeneous metals, whose form is given in Ref. [26]. The shape (3) has been employed in Ref. [19] for a similar study involving classical fluids. The current results are obtained by solving Eq. (1) employing a three-dimensional (3D) code constructed along the same lines as those in Refs. [23,25].

The new aspects of the present calculation are the following. The goal is to find two-dimensional (2D) profiles $\rho(x, z)$ translationally invariant along the y–axis, where the boundary line lies. Useful input material are points of the zero temperature isotherms $\mu(n)$, with $n = \frac{N}{A}$ the areal coverage, for each substrate in Ref. [26], namely alkali metals and Mg. These isotherms are very similar to those shown in Ref. [24], with minor departures due to the different density functionals employed –the current one yielding slightly lower values of chemical potential and grandpotential—and will not be displayed here in view of the long computing times needed to extract smooth curves. The calculation procedure is applied to select values of the chemical potential where films exist on at least two different metals. For each chemical potential, the density profiles of both films are computed separately on the corresponding uniform substrates. These densities identified as ρ_L and ρ_R are placed on the respective left and right halfspace—which extend from $-L_x$ to L_x, joined by a smooth Fermi function in the x–coordinate that creates an initial interfacial profile, and evolved in imaginary time [23,25] to minimize the excess grandpotential per unit transverse length $2\,L_y$

$$\tau_b = \frac{\Delta\Omega}{2L_y} = \int_0^\infty dz \int_{-L_x}^{L_x} dx\ [f[\rho] + (V_s - \mu)\ \rho] - 2L_x\,\frac{\sigma[\rho_L] + \sigma[\rho_R]}{2} \tag{4}$$

Here $\sigma[\rho_{L,R}] \equiv \sigma_{L,R} = \frac{\Omega_{L,R}}{A}$ is the surface tension of each half film at the liquid–vacuum interface and $2\,L_x$ the horizontal length of the computation cell, so that $A = 4\,L_x\,L_y$. Eq. (4) defines the boundary tension.

3 Calculations and Results

The calculations here presented contemplate different compositions of the heterogeneous substrate for values of the chemical potential in the stability region, $\frac{d\mu}{dn} > 0$ and below the bulk figure for helium, $\mu_0 = -7.15$ K. In the range of coverages here considered, weak adsorbers like Cs and K are heliophobic ($\Omega > 0$) while Na, Li and Mg are heliophilic ($\Omega < 0$); in fact, Cs is not wetted by helium at zero temperature, but stable films with negative grandpotential appear on K with a broad prewetting jump, at a much higher coverage [24]. It is to be noted that even for chemical potentials close to the saturation one μ_0, the film cannot be regarded as macroscopic, since the layer structure at the nanoscopic level remains fully visible.

As one samples different combinations of adjoining substrates, the first observation is the fact that the boundary tension is positive indicating an energy cost in order to join the two half films. To identify the characteristics of the boundary tension and their possible relationship to the shape of the interface, it is useful to group the samples according to two criteria: (a) by fixing the chemical potential and considering pairs of the type L–R, as shown in Table 1, and (b) by fixing the L–R pair and varying the chemical potential as seen in Table 2. In both tables, in addition to the value of the boundary tension, other useful data for analyses are listed, such as the total coverage n, the surface tensions of the lateral films, and the absolute value $|\Delta D|$ of the difference between the depths of the substrate potentials in the half spaces from Ref. [26]. As a rule, the strongest adsorber is placed on the left side. The total coverage is constructed by integration of the output density per unit area

$$n = \frac{1}{4L_xL_y} \int_{-L_x}^{L_x} dx \int_{-L_y}^{L_y} dy \int_{0}^{L_z} dz\ \rho(x, y, z) \tag{5}$$

The boundaries of the computation cell have been chosen sufficiently large to secure that the partner films reach their asymptotic profiles, with tests to guarantee that the three-dimensional densities profiles are stable against small modifications of either cell dimension. In other words, the finite size of the computation cell does not impose any spurious strain in the transition region; actually, the displayed calculations employ $L_x = L_y = 80$ Å, while the smooth interfaces occupy 5–10 Å. It should be noted that the total coverage in (5) naturally splits into L and R contributions by considering the corresponding domains in the x–coordinate, however to keep a manageable number of parameters, it is convenient to refer to the global quantity for data analyses.

The first group of data in Table 1 corresponds to $\mu = -8.5$ K with two subgroups for the L adsorber, i.e., Mg or Li. This is close to the prewetting jump for helium on Na at zero temperature as predicted by the current FRDF, and is to be considered the lower boundary for the existence of wetting helium films on this adsorber; other combinations are excluded because for the weaker substrates K and Cs, the films do not exist at this chemical potential. In fact, in such situations the expected density profile is a step–like distribution on the wettable (L) side, thus giving rise to

Table 1 The boundary tension of helium interfaces for the given chemical potentials and substrate compositions, together with areal coverage and surface tensions of the individual half films

$\mu(K)$	Composition	n (Å^{-2})	$\sigma_L(K\text{Å}^{-2})$	$\sigma_R(K\text{Å}^{-2})$	$\lvert\Delta D(K)\rvert$	$\tau_b(K\text{Å}^{-1})$
−8.5	Mg–Na	0.184	−1.846	−0.106	23.093	0.732
	Li–Na	0.151	−0.461	−0.106	5.339	0.218
−7.5	Li–Na	0.297	−0.696	−0.297	5.338	0.117
	Li–K	0.268	−0.696	0.013	9.759	0.606
	Li–Cs	0.254	−0.696	0.083	10.897	1.009
	Na–K	0.243	−0.297	0.013	4.421	0.116
	Na–Cs	0.229	−0.297	0.083	5.559	0.436
	K–Cs	0.200	0.013	0.083	1.137	0.054

The quantity $|\Delta D|$ is the absolute value of the difference between depths of the adsorbing potentials (in K) taken from Ref. [26]

Table 2 Same as in Table 1 for the pair Mg–Li

$\mu(K)$	n (Å^{-2})	$\sigma_L(K\text{Å}^{-2})$	$\sigma_R(K\text{Å}^{-2})$	$\tau_b(K\text{Å}^{-1})$
−7.5	0.354	−2.156	−0.695	0.099
−8.5	0.213	−1.846	−0.461	0.162
−9.0	0.178	−1.736	−0.376	0.305
−10.0	0.146	−1.523	−0.247	0.180
−11.0	0.112	−1.359	−0.140	0.342
−12.0	0.095	−1.014	−0.085	0.599

The difference $|\Delta D|$ takes the value 17.755 K

a singular boundary tension. Figure 1 displays, in the upper panel, the translationally invariant densities $\rho(z)$ for the three adsorbers, while the corresponding mean fields that arise from functional differentiation of the potential energy as seen in Eq. (1)

$$V_{mean}(z) = V\,[\rho(\mathbf{r})] + V_s(z) \tag{6}$$

are shown in the lower panel. The second group in Table 1, in correspondence with the layering profiles and mean fields illustrated in Fig. 2, exhibits data for $\mu = -7.5$ K—close enough to the saturation value—with three subgroups labelled by the strongest adsorber L (e.g., Li, Na or K). Magnesium at −7.5 K is excluded from this list of paired substrates, because as seen in the lower panel of Fig. 2, the mean field decays very slowly, which requests much larger computation boxes. The substrate Rb is not considered in the current calculations, in view of the large similarity between adsorption profiles of helium on this metal and on Cs.

The layering profiles of the adjoining films on their respective homogeneous substrates in Figs. 1 and 2 confirm the expectations that follow from the relative shape and location of the $\mu(n)$ isotherms (cf. Ref. [24]), namely, the stronger the adsorber, the broader the film and the richer the layering structure, whose structure follows the reflection of the mean field with respect to the horizontal axis.

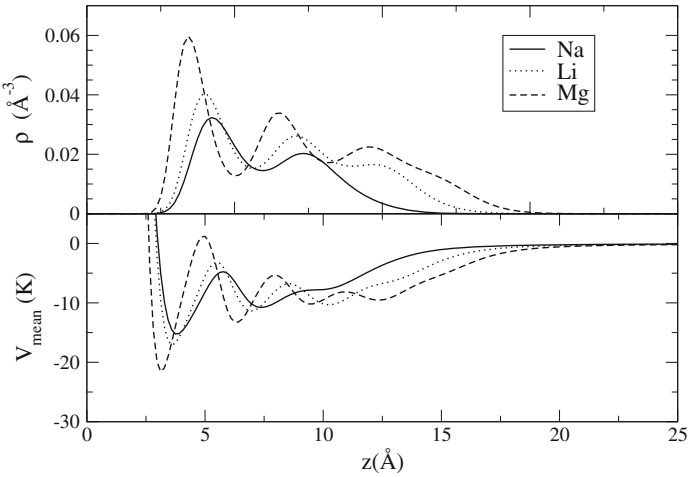

Fig. 1 Density profiles of helium films on homogeneous substrates at $\mu = -8.5$ K.

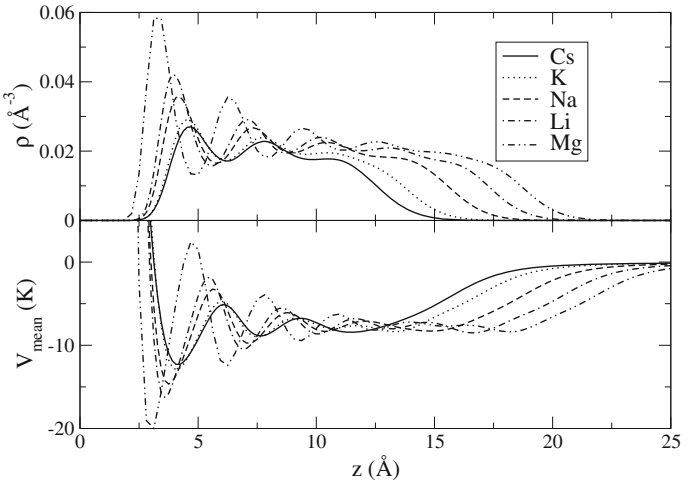

Fig. 2 Density profiles of helium films on homogeneous substrates at $\mu = -7.5$ K.

Starting from type (a) data defined at the beginning of Sec. 3 (fixed chemical potential), from the analyses of Table 1 and examination of Figs. 1 and 2 we can see that for each chemical potencial and composition, the absolute value of the interfacial tension scales with $|\Delta D|$ and with the jump in the lateral spread of the adjoining films. As an illustration, Fig. 3 displays the contour map of $\rho(x, z)$ for the Li–Cs combination, which corresponds to the largest boundary tension in Table 1, with contours to guide the eye. We appreciate the disappearance of two helium layers on Li within a spatial range of nearly 5 Å as seen in Fig. 2. The apparent rule for these boundary tensions is that the energy cost for constructing the interface is essentially associated to the removal of layers from the strongest adsorber. In fact, the smallest values of the boundary tension occur for the combination Li–Na at $\mu = -8.5$ and for the pair K–Cs at $\mu = -7.5$ K,

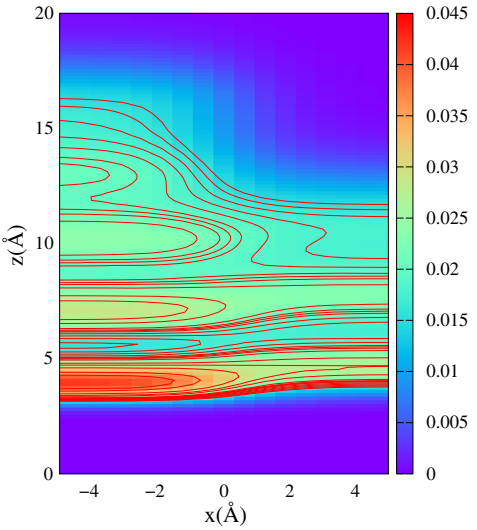

Fig. 3 Interfacial profile of a helium film on a composite Li–Cs substrate at $z = 0$, for chemical potential $\mu = -7.5$ K. Densities on the right column are in Å^{-3} (Color figure online)

where the difference in transverse size of the partners is small as compared to the other pairs.

It is generally understood that an interfacial energy should reveal the competition of the adhesive and cohesive forces acting on the fluid sample, in charge of creating both the mean field and the film shape; however, it is to be noted that at variance with classical fluids, at zero temperature, the quantum pressure associated to the finite kinetic energy of the liquid counteracts to a moderate extent—below 7% of the absolute value of total energy—the overall attraction. To illustrate further the formation of the interface, one can explore the type (b) data for each fixed Mg–Li pair in Table 2. This substrate composition has been selected due to the fact that these are the strongest adsorbers and in spite of the remarkable value of $|\Delta D|$, for both substrates helium presents a prewetting jump not wider than a single monolayer. The case $\mu = -7.5$ K has been included for completeness, at extra computational cost, and the lowest chemical potential equal to -12 K is near the prewetting value for submonolayer condensation of helium on Li. Figure 4 shows six panels corresponding to the Mg–Li combination for values of the chemical potentials in the range $[-12K, -7.5K]$. In each plot, the left (right) panel displays the asymptotic profile $\rho(z)$ that coincides with that for the translationally invariant density on the respective homogeneous surface, while the middle panel is a contour plot for the profile $\rho(x, z)$.

Although seemingly redundant, these plots are useful to elucidate some trends for the boundary tension dissociated from its dependence on the relative adsorption strength as in type (a) data. One may note, in addition, that no obvious relationship between boundary tension and chemical potential, or coverage, can be traced out of the data in Table 2; in fact, the nonmonotonic dependence of τ_b with these magnitudes appears somehow puzzling. The largest boundary tension corresponds to -12 K and occurs for a very thin film with a single monolayer on the Li side and two on Mg; the undergoing process can be visualized as the bifurcation of a single peak on the softer Li surface into two more strongly bound bumps on the harder Mg one. The energy

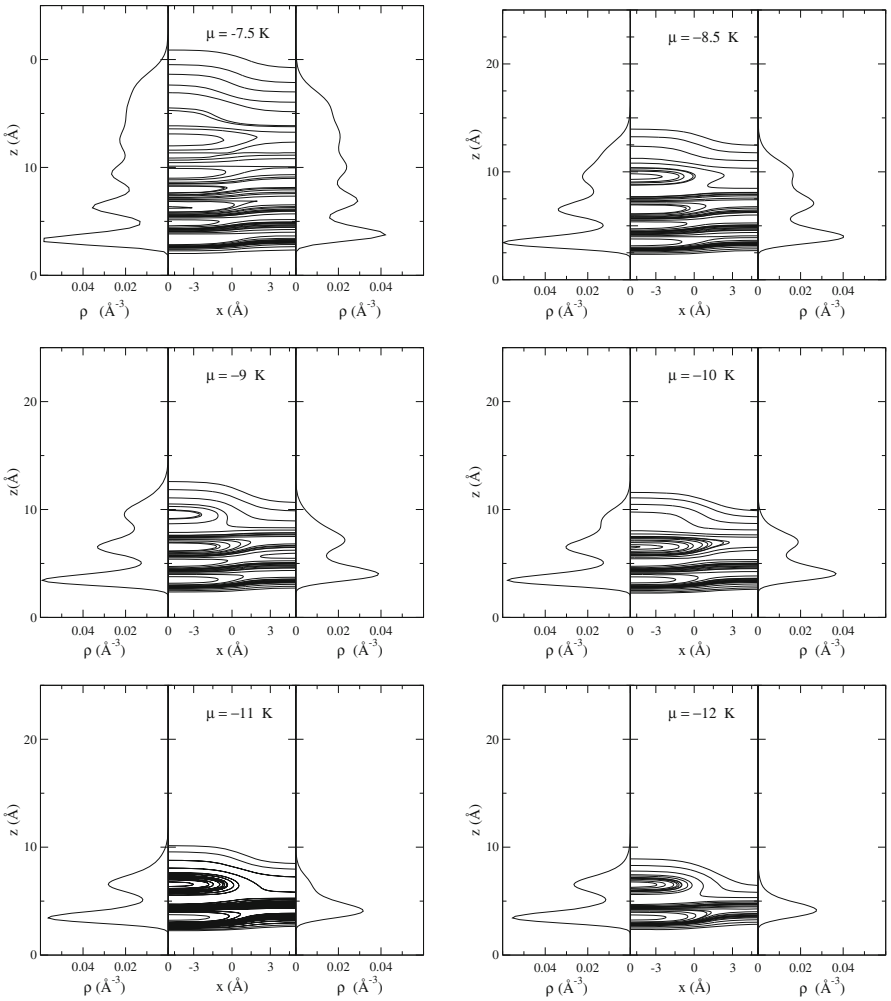

Fig. 4 Sequence of density profiles of helium on homogeneous Mg (L) and Li (R) substrates and interface at the juncture between the two metals for the chemical potentials in Table 2

cost of this construction is reduced when the total amount of deposited helium atoms increases, reaching its smallest value for −10 K where the profiles of the two films are similar, considering that the third peak on the Mg side is not fully developed. This peak is clearly visible at −9 K, where both the structure and the energy cost resemble the lower panel, confirming that an energy supply has to be provided to remove one complete layer formed on the stronger substrate. Comparable profiles already appear at −8.5 K with reduced interfacial energy; the latter is significantly reduced at −7.5 K, when both films approach the bulk limit.

Finally, the magnitude of the boundary tension lies in the range 10^{-1}–1 K/Å, i.e. 10^{-13} to 10^{-12} N in agreement with the lower edge of the scale reported for classical fluids.

4 Summary

This paper reports the first calculation of the interfacial profile and energetics for nanoscopical films of superfluid helium, on an heterogeneous planar substrate consisting of two adjoining metals. The calculations are performed in the frame of grand canonical DFT for the zero temperature case. The possibility of nucleation of finite helium samples [23], that are only stable in a canonical frame, has been deliberately excluded in the present work.

A key feature of the application of FRDF to a quantum fluid is the possibility, here exploited, of restricting oneself to zero temperature, with considerable numerical simplification; in fact, for a quantum fluid such as ^{4}He, one expects that such a description yields acceptable references for realistic systems up to 10^{-2}to10^{-1} K. At variance with classical fluids, an heterogeneous bosonic system possesses a finite kinetic energy, that takes part as well in the establishment of the bundary tension, in the form of a quantum pressure that counteracts the effects of attractive forces. As in most studies of helium under external confinement, the major interest resides on revealing aspects of the structure at the nanoscopic level, and of the involved energetic balance. In this respect, the problem here proposed permits to investigate phenomena that involve the displacement of planar layers of helium across the juncture between the two adjoining substrates, thus bringing into evidence the competition of the various forces –including the quantum pressure– that together give rise to the sign and magnitude of the interfacial tension. The overall scenario agrees with early predictions based on interfacial Hamiltonian models, whose local version relies on capillarity theory [17] where all cohesive effects appear embodied in the surface tension, and where the local film height results from the competition between capillary and substrate forces. Since this view has been devised for macroscopic films, doubts might arise regarding its validity for systems of nanoscopic size, especially for those films with a noticeable shell structure, thus the convenience of employing a more sophisticated instrument like a fully 2D or 3D FRDF code.

A possible limitation of the current approach may be the fact that the substrate potential is a function of the transverse coordinate only; in other words, each helium atom feels only the effect of the substrate at its (x, y) location, while in a realistic situation every particle is exposed to the whole heterogeneous adsorber. This drawback could be removed by the use of a potential depending on both x and z, such as the one in Ref. [17], to the expense of much larger computing times for each sample. The possibility of undertaking a more refined calculation along these lines remains open. In addition, future developments of this work point to the study of helium on Cs, a widely investigated system, both on theoretical and experimental standpoints; however, a calculation of the coexisting profile at finite temperatures on an homogeneous substrate poses a very important numerical effort, currently under consideration [27].

Acknowledgments The author is thankful to F. Ancilotto, M. Barranco and M. Pi for interesting conversations and for many valuable computational hints, and to M. Cole for critical comments. This work was performed with partial support from Grants PIP 0546 from CONICET, UBACYT 01/K156 from University of Buenos Aires and PICT 2011/1217 from ANPCYT, Argentina.

References

1. P. de Gennes, Rev. Mod. Phys. **57**, 827 (1985)
2. D. Bonn, D. Ross, Rep. Prog. Phys. **64**, 1085 (2001)
3. B.M. Law, Prog. Surf. Sci. **66**, 159 (2001)
4. J.W. Cahn, J. Chem. Phys. **66**, 3667 (1977)
5. C. Ebner, W.F. Saam, Phys. Rev. Lett. **38**, 1486 (1977)
6. B. Widom, A.S. Clarke, Phys. A **168**, 149 (1990)
7. J. W. Gibbs, The Scientific Papers of J. W. Gibbs, vol 1, p. 288, Dover, N. Y., 1961.
8. J.O. Indekeu, Physica A **183**, 439 (1992)
9. E.M. Blokhuis, Physica A **202**, 402 (1994)
10. J.O. Indekeu, Int. J. Mod. Phys. B **8**, 309 (1994)
11. J.Y. Wang, S. Betelu, B.M. Law, Phys. Rev. E **63**, 031601 (2001)
12. A. Amirfazli, A.W. Neumann, Adv. Colloid Interface Sci. **110**, 121 (2004)
13. P. Lenz, R. Lipowsky, Phys. Rev. Lett. **80**, 1920 (1998)
14. C. Bauer, S. Dietrich, Phys. Rev. E **60**, 69129 (1999)
15. K. Kargupta, A. Sharma, Phys. Rev. Lett. **86**, 4536 (2001)
16. P. Lenz, C. Bechinger, C. Schäfle, P. Leiderer, R. Lipowsky, Langmuir **2001**, 17 (2001)
17. M.W. Cole, E. Vittorators, J. Low Temp. Phys. **22**, 223 (1976)
18. R. Evans, Adv. Phys. **28**, 143 (1979)
19. W. Koch, S. Dietrich, M. Napiórkowski, Phys. Rev. E **51**, 3300 (1995)
20. T. Getta, S. Dietrich, Phys. Rev. E **57**, 655 (1998)
21. C. Bauer, S. Dietrich, Eur. Phys. J B **10**, 767 (1999)
22. F. Ancilotto, F. Faccin, F. Toigo, Phys. Rev. B **62**, 17035 (2000)
23. F. Ancilotto, M. Barranco, E.S. Hernández, A. Hernando, M. Pi, Phys. Rev. B **79**, 104514 (2009)
24. M. Barranco, M. Guilleumas, E.S. Hernández, R. Mayol, M. Pi, L. Szybisz, Phys. Rev. B **68**, 024515 (2003)
25. F. Ancilotto, M. Barranco, E.S. Hernández, M. Pi, J. Low Temp. Phys. **157**, 174 (2009)
26. A. Chizmeshya, M.W. Cole, E. Zaremba, J. Low Temp. Phys. **110**, 677 (1998)
27. M. Pi, private communication.